Journal of Atmospheric and Solar-Terrestrial Physics 80 (2012) 48–59

Contents lists available at SciVerse ScienceDirect

Journal of Atmospheric and Solar-Terrestrial Physics

journal homepage: www.elsevier.com/locate/jastp

The GUMICS-4 global MHD magnetosphere–ionosphere coupling simulation

P. Janhunen [a,*], M. Palmroth [a], T. Laitinen [a], I. Honkonen [a,b], L. Juusola [a], G. Facskó [a,c], T.I. Pulkkinen [d]

[a] Finnish Meteorological Institute, Helsinki, Finland
[b] University of Helsinki, Department of Physics, Helsinki, Finland
[c] Geodetic and Geophysical Institute, Research Centre for Astronomy and Earth Sciences, Hungarian Academy of Sciences, Sopron, Hungary
[d] School of Electrical Engineering, Aalto University, Espoo, Finland

ARTICLE INFO

Article history:
Received 18 October 2011
Received in revised form
21 February 2012
Accepted 10 March 2012
Available online 22 March 2012

Keywords:
Magnetosphere
Modelling
Global MHD simulation
Numerical simulation

ABSTRACT

GUMICS-4 is a global magnetosphere–ionosphere coupling simulation based on global MHD magnetosphere and an electrostatic ionosphere. Here we review the development history, design and technical features of GUMICS-4 as well as a number of its postprocessing tools. We also compare GUMICS-4 predictions with observations for magnetopause distance, interplantary magnetic field penetration in the magnetotail, ionospheric field-aligned current pattern and other quantities. Based on the comparisons we can conclude that to a useful extent and with certain limitations, GUMICS-4 can reveal the detailed spatiotemporal behaviour of the magnetosphere–ionosphere system under given solar wind forcing.

1. Introduction

Plasma dynamics in the Earth's space environment is driven by the solar wind and interplanetary magnetic field (IMF) impinging the Sunward boundary of the internal geomagnetic field. Plasma and energy entry from the solar wind into the magnetosphere occur mainly through magnetic reconnection (Dungey, 1961), but also viscous-like processes may play a role especially at times when the magnetic geometry is not favourable for reconnection (Axford and Hines, 1961).

Modelling the plasma dynamics in the magnetosphere requires accurate treatment of the solar wind driver and its interaction with the magnetospheric field and plasma, as well as dynamics within the different plasma populations in the magnetosphere and their coupling to the ionosphere. Given the large size of the region, the magnetohydrodynamic (MHD) plasma description has usually been adopted to self-consistently treat the entire system.

Developing and running a global MHD simulation of the solar wind – magnetosphere – ionosphere system requires significant development effort as well as computing resources. Even after 20 years of development, there are only a handful of global MHD models that regularly produce results in the published literature. The most widely known codes include the Lyon–Fedder–Mobarry (LFM) model (Lyon et al., 2004), the Space Weather Modelling Framework (SWMF) (Toth et al., 2005) which is built around the BATS-R-US MHD core (Powell et al., 1999), the Open General Geospace Circulation Model (OpenGGCM) (Raeder et al., 2008), the Ogino model (Ogino et al., 1994) and the Grand Unified Magnetosphere–Ionosphere Coupling Simulation (GUMICS).

Simulation runs can be performed either by artificial solar wind input or by actual time series of measured solar wind and interplanetary field parameters. The artificial input allows one to examine the flow of processes under simplified conditions in order to study causal relationships and/or code behaviour under given circumstances. On the other hand, realistic solar wind input produces time series of the dynamics, which then can be compared with observations in various parts of the magnetosphere – ionosphere system to verify the code performance and to examine the key processes during specific events.

While there have been attempts to evaluate the performance of the various codes, for example the reconnection challenge examining local MHD, hybrid and particle simulations in reconnection geometry (Birn et al., 2001) or the modelling challenge on global models (Pulkkinen et al., 2010), the answers have often been inconclusive. The codes are different rather than organised in an absolute scale of quality, and often enough we do not have sufficient observations to adequately assess the model performance. For instance, comparing against single-spacecraft time series means comparing a single trace in a 4-D space, where even a slightly different geometry leads to vastly different results even if the large-scale properties were accurately reproduced. Global observations often come from multiple sources, from the ionosphere outside the MHD domain, or from indirect measurements making conversion to plasma physical parameters inaccurate.

* Corresponding author. Tel.: +358 9 19294635; fax: +358 9 19294603.
E-mail address: pekka.janhunen@fmi.fi (P. Janhunen).

1364-6826/$ - see front matter © 2012 Elsevier Ltd. All rights reserved.
http://dx.doi.org/10.1016/j.jastp.2012.03.006

The code complexity, continuous development of the models and the fact that it is impossible to document all the details of the codes in scientific journals has produced further complications to comparisons and evaluations of the models. Due to the different code setups, runs even with the same code are not necessarily directly comparable (Ridley et al., 2010), and thus all comparisons require detailed expertise from the modelling group itself. The Community Coordinated Modeling Center (CCMC) run by NASA (http://ccmc.gsfc.nasa.gov/) has improved the situation by allowing users to run several models in a user-defined setup.

From early on, the modellers as well as the model users realised that non-MHD processes especially in the inner magnetosphere lead to significant differences between the model output and observations. While some models have acknowledged this as a fact, others have taken the route to couple a variety of other plasma models to the MHD domain to represent the missing part of the physics in some parametrised way. Especially the LFM (Wang et al., 2004; Toffoletto et al., 2004) and the SWMF (De Zeeuw et al., 2004) models can be run in a setup that couples models that account for as well ionospheric and atmospheric processes as multiple plasma components in the inner magnetosphere. The disadvantage of using the coupled option is the added complexity; it becomes more challenging to identify the causal relationships and physical processes that account for the dynamics in the system.

The GUMICS-4 model has an electrostatic ionosphere, but no separate inner magnetosphere module. The code has remained unchanged for several years, the advantage of which is that the results are comparable with each other because only one code version was used to generate them. All parameters and settings affecting the results are given in the parameter input file, and stored with the run results. Thus, runs appearing in published papers differ only in the solar wind input and (rarely) the maximum grid adaptation level defining the minimum cell size. The solar EUV flux, parameterised by the measured solar radio F10.7 cm flux, appears as a constant in GUMICS source code and it has thus far not been modified in published runs. Therefore, almost all runs published from the GUMICS-4 model are mutually comparable.

The purpose of this paper is to document the properties and the development history of the GUMICS-4 global magnetohydrodynamic simulation of the coupled solar wind – magnetosphere – ionosphere system. The aim is to include more of the technical model details than is usually possible in a regular research paper. In addition to the code description, we document the quantitative analysis methods that have been developed for the analysis of the simulation results. Based on these results, we review the general properties of the GUMICS-4 solutions and conclude by an outlook to the future development of the model.

2. GUMICS-4 code

2.1. Development history

Different from most other global MHD-based ionosphere–magnetosphere coupling simulations, GUMICS was developed "inside out", i.e. from the ionosphere towards the magnetosphere. The insights to ionospheric physics of the EISCAT radar community were important for the development of the ionospheric part of the original GUMICS. Even the name GUMICS ("Grand Unified Magnetosphere Ionosphere Coupling Simulation") was chosen to continue the "GU" line of the EISCAT software and analysis tools. The name GUMICS was only sporadically used until GUMICS-3, but because the work progressed in four clear stages we label them GUMICS-1 to GUMICS-4 here.

GUMICS-1 had a mesoscale ($\sim$1000 km) planar Cartesian ionosphere simulation box coupled to a 2-D slab of MHD fluid layer (Janhunen and Huuskonen, 1993). The ionospheric model solved the elliptic equation coming from current continuity. The height-integrated Pedersen and Hall conductivities were let depend on the electron precipitation. A central ionosphere–magnetosphere coupling agent was the field-aligned current (FAC) which was related to the fluid vorticity in the MHD slab. At equation level, the GUMICS-1 setup largely followed an earlier work of Lotko and Schultz (1987). GUMICS-1 ran on the Cray X-MP vector machine and was written in C.

In GUMICS-2 the ionospheric model was transferred from Cartesian to spherical coordinates to allow larger spatial scales to be considered (Janhunen et al., 1995). At the same time, the 2-D incompressible magnetosphere was replaced by a 3-D compressible full MHD magnetosphere. The simulation box consisted of the nightside auroral ionosphere and a subregion of the magnetotail that was magnetically mapped to it. The MHD part was embedded within a magnetosphere modelled by the Tsyganenko-89 field model and various simple analytic models were used for the plasma pressure and density. Near the boundaries of the MHD box, the external, analytic models were gradually mixed with the MHD solution to mitigate boundary effects. The employed MHD solver was simplistic and the MHD grid was uniform. Issues with the boundary conditions and the simplistic MHD solver precluded GUMICS-2 from being used in actual scientific work.

These shortcomings were addressed in GUMICS-3 (Janhunen, 1996). To get rid of the cumbersome internal boundaries, in GUMICS-3 the geometry was made global, and the Tanaka (1994) formulation of a Godunov-type MHD solver was implemented. At the same time the programming language was changed from C to C++. As the MHD simulation box had grown in size, an adapted grid was implemented for acceptable running times on a vector machine. Temporal subcycling was introduced to further increase the performance. Vectorisation of the adapted grid solver was accomplished by precomputed index vectors containing the grid cell neighbourhood information as well as cell "time classes" computed from local Courant conditions. The adapted grid was generated as a preprocessing step in Tela numerical scripting language (http://www.space.fmi.fi/prog/tela.html) which was also used for postprocessing. This reduced the programming effort because Tela code is easier to write than C++.

In principle, GUMICS-3 worked well: it employed an adapted grid and temporal subcycling and it ran at nearly optimal megaflops rating on the then fastest computer, the Cray C-90. Its main shortcoming was that the grid adaptation did not respond dynamically to solar wind changes. It turned out (which is natural in retrospect) that to get an accurate solution, the adapted refinement must be exactly and not only approximately at the right place (for example at the magnetopause or other discontinuity). Another drawback of GUMICS-3 was a spherical coordinate singularity at the poles in the ionospheric solver, but that was more a nuisance than a serious problem.

In 1996–1997, vector supercomputers started to become extinct. This was a crisis for GUMICS. On one hand, GUMICS-3 had demonstrated (with clever use of hardware and software possibilities of the time) that it is very nearly possible to run simulations with useful accuracy, but on the other hand the adopted line of development was becoming a computing technological dead end. It was seen that the next version of GUMICS had to run on a personal computer (PC). That implied a drastic drop in performance compared to C-90 no matter how it was done, but the effect had to be mitigated as much as possible.

GUMICS-4 (i.e. the present version which is the subject of this paper) was developed to address these issues. The majority of the

development took place 1997–1998 and was completed in 2000, with some small fixes taking place later. The development of GUMICS-4 from GUMICS-3 proceeded as follows. (1) The MHD grid was rewritten in C++ and automatic runtime grid adaptation was implemented. (2) The ionosphere was rewritten in a coordinate-free finite element form to eliminate spherical coordinate singularities at the poles. (3) The HC (Hierarchical Cartesian) file format was designed to store adapted MHD grids and the postprocessing programme `hcvis` was written to read and display those files efficiently. (4) To facilitate 1-D and 2-D validation tests, the MHD part was developed into a general-purpose one and a separate hydrodynamic solver option was added. The transition from GUMICS-3 to GUMICS-4 was hence rather straightforward, although laborious.

The long-term motivation for developing GUMICS was to gain insights of the processes within the magnetosphere–ionosphere system during dynamic events such as substorms. The intermediate models before GUMICS-4 were all successful demonstrations of certain aspects of the problem. GUMICS-4 became a success and its results have been used in many publications, probably because to a useful extent, it reveals what happens in the magnetosphere–ionosphere system during dynamic events.

2.2. MHD solvers

GUMICS-4 uses a first order finite volume method written in the conservative variables $(\rho,\rho\mathbf{v},U,\mathbf{B})$ where ρ is the plasma mass density, $\mathbf{v}$ is the velocity, U is the total energy density and $\mathbf{B}$ is the magnetic field. It also uses analytic separation out of the dipole field $\mathbf{B}=\mathbf{B}_0+\mathbf{B}_1$ (Tanaka, 1994). With this separation the ideal MHD equations solved by GUMICS-4 are given by

$$\frac{\partial\rho}{\partial t}=-\nabla\cdot\mathbf{p}$$

$$\frac{\partial\mathbf{p}}{\partial t}=-\nabla\cdot\left[\frac{\mathbf{pp}}{\rho}+\left(P+\frac{B^2}{2\mu_0}-\frac{B_0^2}{2\mu_0}\right)\mathrm{I}-\frac{1}{\mu_0}(\mathbf{BB}-\mathbf{B}_0\mathbf{B}_0)\right]$$

$$\frac{\partial U_1}{\partial t}=-\nabla\cdot\left[\left(U_1+P+\frac{B_1^2}{2\mu_0}\right)\frac{\mathbf{p}}{\rho}-\frac{\mathbf{B}_1(\mathbf{p}\cdot\mathbf{B}_1)}{\mu_0\rho}+\frac{\mathbf{B}_1\times(\mathbf{p}\times\mathbf{B}_0)}{\mu_0\rho}\right]$$

$$\frac{\partial\mathbf{B}_1}{\partial t}=\nabla\times\left(\frac{\mathbf{p}\times\mathbf{B}}{\rho}\right) \tag{1}$$

where $\mathbf{p}=\rho\mathbf{v}$ is the momentum density, I is the unit dyad and U_1 is the total energy density from which the dipole contribution has been subtracted, $U_1=U-(\mathbf{B}_1\cdot\mathbf{B}_0)/\mu_0-B_0^2/(2\mu_0)$. The total energy density U is given by $U=P/(\gamma-1)+p^2/(2\rho)+B^2/(2\mu_0)$. The relationship between U_1 and the pressure P is $P=(\gamma-1)(U_1-p^2/(2\rho)-B_1^2/(2\mu_0))$. The benefit of the splitting $\mathbf{B}=\mathbf{B}_0+\mathbf{B}_1$ is that one does not have to subtract the large quantity $B_0^2/(2\mu_0)$ from U when computing the pressure, thus making it numerically less challenging to maintain positive pressure.

GUMICS-4 uses primarily Roe's approximate Riemann solver (Roe, 1981). The intermediate states returned as a byproduct of computing the Roe solver are checked for physicality (positive density and pressure) and if any of the states is nonphysical, the robust although diffusive Harten–Lax–van Leer (HLL) solver (Harten et al., 1983) is used instead of the Roe solver for that interface and timestep. Of the existing global MHD models, the SWMF (Ridley et al., 2010) is most similar to GUMICS, and there was a lot of information exchange between SWMF and GUMICS during development. Among the main differences between GUMICS and SWMF are that SWMF uses block adaption instead of cell by cell adaptation, is parallelised, uses second order method and that it does not use temporal subcycling.

GUMICS-4 uses a first order Godunov-type scheme primarily because a higher order scheme would be cumbersome to use together with temporal subcycling when adaptive mesh refinement is also in employed. While classical first order schemes such as Lax-Fridrichs are quite diffusive, in Godunov-type schemes the amount of diffusion for a propagating wave is proportional to its propagation speed. The first-order Godunov-type scheme used by GUMICS-4 has large diffusion for waves moving rapidly across the grid, but for slow moving structures such as the magnetopause, bow shock and tail current sheet the diffusion is small. Indeed, said structures are resolved by only a few grid spacings in GUMICS which is almost optimal for any numerical scheme.

The 7-wave Riemann solver used preserves $\nabla\cdot\mathbf{B}=0$ to truncation error, but the divergence tends to accumulate over long time so it must be periodically removed. This is done in GUMICS-4 by the projection method (Brackbill and Barnes, 1980), i.e. by replacing $\mathbf{B}$ by $\mathbf{B}'=\mathbf{B}+\nabla\psi$, demanding $\nabla\cdot\mathbf{B}'=0$ and solving the resulting Poisson equation $-\nabla^2\psi=\nabla\cdot\mathbf{B}$ for ψ. The 3-D Poisson equation on the unstructured grid is solved by the iterative conjugate gradient method (Press et al., 1992). The divergence removal step is performed every 20 s of simulation time and typically uses $\sim 10\%$ of the computing time.

Various reasons can cause the pressure in some cell to become negative in conservative scheme MHD simulations, see Janhunen (2000) for an exposition of the issue. If that happens, the previous cell state (which still had positive pressure) is linearly mixed with the updated one until the pressure becomes marginally positive. This procedure breaks the conservation laws locally when invoked, but is usually able to treat the problem so that the run can continue. In our experience, if a negative pressure is not fixed immediately, the problem has a tendency to get worse and to ruin the computation.

2.3. Adaptive grid and temporal subcycling

The grid used by GUMICS-4 is a cell-by-cell refined hierarchically adaptive octogrid. The top level has a basegrid consisting of $(8R_E)^3$ cells which are refined when needed. For refining the grid, a refinement index is computed for each cell. The refinement index α is computed as a maximum of several terms containing dimensionless gradients of MHD variables:

$$\alpha=\max\left(\frac{\Delta\rho}{\widehat{\rho}},\frac{\Delta U_1}{\widehat{U_1}},\frac{(\Delta\mathbf{p})^2}{2\rho\widehat{U_1}},\frac{(\Delta\mathbf{B}_1)^2}{2\mu_0\widehat{U_1}},\frac{|\Delta\mathbf{B}_1|}{\widehat{B_1}}\right) \tag{2}$$

where Δ denotes difference between the neighbouring cells in question and the hat denotes their maximum. If the refinement index exceeds a threshold, the cell is refined, i.e. broken down into eight children cells that are initialised with copies of the parent's MHD data (i.e. zeroth order interpolation is used when filling the children cells). If the refinement index drops below another (smaller) threshold in all children cells of a parent cell, the parent cell is recoarsened by averaging the children data into it and deleting the children. When refining, each child cell receives a copy of the parent cells' data values. When recoarsening, the children data are arithmetically averaged to form the parent cell data. Refinement may be done up to a maximum specified adaptation level which is usually 5, corresponding to $0.25R_E$ minimum cell size and typically of the order of 400,000 grid cells (the number of cells varies during the run because of dynamic adaptation).

The condition that the adaptation level may change only by ± 1 between neighbouring cells is strictly imposed, i.e. the grid is properly nested. For this purpose, refining one cell may induce the need to refine potentially a large number of neighbouring cells. A recursive algorithm is used to implement these induced

refinements when needed. Because the method is first order, the neighbouring cell values are used in the interface flux computations directly regardless of their sizes.

In addition to the global maximum adaptation level, local minimum and maximum cell size are defined throughout the simulation box as analytic functions. Also the refinement and recoarsening index thresholds depend on location such that the near-Earth region and the magnetotail get the highest emphasis. In this setup the grid adaptation scheme is semiautomatic, i.e. it runs automatically based on gradient information obtained from the solution, but also depends on the user-definable analytic functions. This is essential for performance. If the code would be allowed to refine everything with the same criteria, it would tend to refine e.g. the entire magnetopause to the maximum resolution which would easily generate a much larger number of grid points than the default version without much improving the accuracy in the near-Earth region. The primary goal of GUMICS is to model ionosphere–magnetosphere coupling, so a fully accurate representation of e.g. the distant magnetopause is not needed because it is not essential for modelling the near-Earth region well.

Temporal subcycling is used to speed up the computation. A base timestep (called *time leap*) of ΔT ($=1$ s by default) is divided by two until the local Courant condition is satisfied. Thus for each cell, the timestep is one of the 1 s, 0.5 s, 0.25 s, 0.125 s, …. For each cell we define a *timeclass* n such that the local timestep is $\Delta t = \Delta T/2^n$. The timeclasses are recomputed at the beginning of each time leap based on the local Courant conditions. The timeclasses are processed in certain order which guarantees that initial data from the neighbours (in spirit of the forward Euler method) are available when the processing of the timeclass starts. The order in which the cells are propagated within each timeclass is free.

In theory, temporal subcycling could cause an instability if the actual Courant condition changes so much during one timeleap that the timestep that was computed for some cell at the beginning of the leap is no longer stable. To reduce the probability of this occurring, a safety factor (by default 0.8) is used in the Courant condition when computing the timeclasses.

Temporal subcycling is quite helpful in reducing the computational work for magnetospheric MHD simulations. This is because the strongly nonuniform dipole field forces the timesteps to be very short only in the near-Earth region while they can be much larger elsewhere. If global time stepping was used, the small timesteps would have to be used everywhere.

2.4. Ionosphere and magnetosphere–ionosphere coupling

The ionosphere is modelled as a spherical surface with radially integrated current continuity:

$$\nabla \cdot \mathbf{J} = \nabla \cdot [\boldsymbol{\Sigma} \cdot (-\nabla \Phi + \mathbf{v}_n \times \mathbf{B})] = -j_{\parallel}(\hat{\mathbf{b}} \cdot \hat{\mathbf{r}}) \tag{3}$$

where $\boldsymbol{\Sigma}$ is the height-integrated conductivity tensor, Φ is the ionospheric potential, $\mathbf{v}_n$ is the neutral wind (taken equal to Earth's rotational speed), $j_{\parallel}$ is the field-aligned current and $\hat{\mathbf{b}} \cdot \hat{\mathbf{r}}$ is the cosine of the angle between the magnetic field direction $\hat{\mathbf{b}}$ and the radial direction $\hat{\mathbf{r}}$. The height-integrated conductivity tensor is defined by its action on any electric field $\mathbf{E}$ as

$$\boldsymbol{\Sigma} \cdot \mathbf{E} = \Sigma_P \mathbf{E} + \Sigma_H \hat{\mathbf{b}} \times \mathbf{E} \tag{4}$$

where $\Sigma_{P,H}$ is the height-integrated Pedersen and Hall conductivity, respectively.

Eq. (3) is an elliptic equation with variable coefficients for Φ. We discretise the ionospheric plane (a spherical surface) with triangles. The triangulation starts from the icosahedron and each face is recursively refined according to a prescribed grid density function. The grid is densest in the auroral oval (about 180 km spacing) and rather dense (360 km spacing) in the polar caps. Thus the ionospheric grid is unstructured and adapted at the start, but the adaptation stays constant during the run. Eq. (3) is solved by the conjugate gradient algorithm (Press et al., 1992).

The finite element formulation is used for discretising the elliptic equation (3). This makes the solver coordinate-free so that although the surface where the equation is solved is a sphere, spherical or other curvilinear coordinates are not used so that one trivially avoids the issues of coordinate singularities at the poles. Because the whole ionosphere including the equatorial region is solved, there is no need for any boundary conditions except to fix the arbitrary constant that can be added to the potential (a sphere has no boundaries). The only inputs to the ionosphere are fed from the magnetosphere through the field-aligned current, electron precipitation and solar EUV ionisation.

The height-integrated conductivities are obtained from

$$\Sigma_{P,H} = \sqrt{(\Sigma_{P,H}^{\mathrm{ele}})^2 + (\Sigma_{P,H}^{\mathrm{UV}})^2} \tag{5}$$

where the terms labelled by "ele" and "UV" are the contributions due to electron precipitation and solar UV radiation, respectively. Standard trick of square summing is used for conductivities because the ionisation production rates add linearly while the electron density squared (and thus the conductivity squared) is proportional to the production rate in a stationary state. For the solar UV contributions, the empirical formulas of Moen and Brekke (1993) are used:

$$\Sigma_P^{\mathrm{UV}} = 0.5 \text{ mho} + F_{10.7}^{0.49}(0.34 \cos\chi + 0.93\sqrt{\cos\chi}) \text{ mho}$$

$$\Sigma_H^{\mathrm{UV}} = 0.5 \text{ mho} + F_{10.7}^{0.53}(0.81 \cos\chi + 0.54\sqrt{\cos\chi}) \text{ mho}. \tag{6}$$

Here $F_{10.7}$ is the 10.7 cm solar radio flux which is used as a proxy for solar UV activity, and χ is the solar zenith angle. In GUMICS-4 the 10.7 cm (2800 MHz) radio flux is a source code constant whose standard value is 100×10^{-22} W m^{-2}. The term 0.5 mho is added to model the background ionisation due to stellar UV and cosmic rays. The solution gains dynamics (starts to display more complex behaviour) and finally becomes unstable if one artificially sets the Pedersen conductivity very small, thus the base value of the conductivity is not an irrelevant parameter.

The electron precipitation contributions to $\Sigma_{P,H}$ are obtained by height integration from the corresponding 3-D quantities $\sigma_{P,H}$ which are in turn obtained by textbook formulas (models for the required electron-neutral and ion-neutral collision frequencies are obtained from the MSIS model Hedin, 1991) from the 3-D ionospheric electron density n_e due to precipitation. The latter is solved from its continuity equation:

$$\frac{\partial n_e}{\partial t} = q - \alpha n_e^2 \tag{7}$$

where q is the ionisation production rate due to electron precipitation and α is the recombination constant ($\alpha = 3 \times 10^{-13}$ m^3/s).

The ionospheric field-aligned current and potential are mapped with dipole mapping to the $3.7R_E$ sphere which is the inner boundary of the MHD domain. The ionosphere–magnetosphere potential difference is zero by default.

Electron precipitation particle flux is computed as the thermal electron flux from the MHD plasma by assuming an ion to electron temperature ratio of 4. Before using the MHD density in the electron precipitation computation, it is multiplied by the loss cone filling rate. The loss cone filling rate χ_{LCFR} is taken to be

$$\chi_{\mathrm{LCFR}} = 0.01 + 0.99 \cdot \frac{1}{2}\left[1 + \tanh\left(\frac{23^\circ - \theta}{6^\circ}\right)\right] \tag{8}$$

where θ is the magnetic colatitude ($0 \le \theta \le 90^\circ$, measured from the nearest pole). The loss cone filling rate is almost unity inside the polar cap and goes smoothly to almost zero when the magnetic

latitude decreases from 70° to 60°. Including χ_{LCFR} is quite necessary because without it, GUMICS-4 would predict bright aurora nearly all the time at subauroral latitudes such as in Helsinki. The *ad hoc* form of Eq. (8) is less than perfect, but modelling the loss cone filling rate in some self-consistent way would not be straightforward in the MHD framework.

2.5. Boundary conditions

The simulation box extends from -224 to $+32R_E$ in x and from -64 to $+64R_E$ in y and z. Neumann boundary conditions are applied to all MHD variables at the outer boundaries of the box, i.e. all values are copied after every timestep from the interior cell to the neighbouring ghost cell. However, at the solar wind inflow boundary $x=+32R_E$, Dirichlet conditions are applied (all values set in the ghost cells by the solar wind input).

The inner boundary is set at $3.7R_E$. There we copy ρ, P, $v_{\parallel}$ and $\mathbf{B}_1$ along the $\mathbf{B}_0$ field line from interior to ghost cells, i.e. we assume that these quantities are constant along the (unperturbed) field line. The velocity perpendicular to B_0 is computed as $\mathbf{v}_{\perp}=\mathbf{E}\times\mathbf{B}/B^2$ where $E=-\nabla\Phi$ and Φ is copied along dipole field from the ionospheric plane (the solution of the elliptic equation in the ionosphere). The ionosphere is recomputed and $\mathbf{v}_{\perp}$ updated at every fourth time leap, i.e. at every 4 s.

2.6. Result files and visualisation

GUMICS-4 writes its output to custom format binary HC (Hierarchical Cartesian) files containing the MHD variables stored in the unstructured octogrid. The HC files are readable by `hcvis` display programme which uses Tcl/Tk for its graphical user interface, C++ for computing and OpenGL for drawing (the Togl interface piece is used to enable OpenGL drawing from Tcl/Tk). There are also some command line utilities for processing HC files, most notably `hcintpol` for interpolating MHD quantities from HC files at arbitrary points. With `hcintpol` it is easy to write programmes in any language that are able to display and postprocess GUMICS-4 outputs. Furthermore, converters to other file formats for HC files exist which enable the use of third-party visualisation software (Honkonen et al., 2011), e.g. VisIt (https://wci.llnl.gov/codes/visit/). An example of `hvcis` screen dump is shown in Fig. 1. The plasma pressure is colour coded and 0.4 nPa pressure isosurface is also drawn, together with flowlines from the solar wind boundary and traces of the nightside magnetic field.

The ionospheric data (potential, height-integrated conductivities, etc.) are written in separate ionospheric files that are also of a custom binary format. There is a separate OpenGL/GLUT based programme `ionovis` for displaying ionospheric data and `ionointpol` for interpolating to arbitrary location.

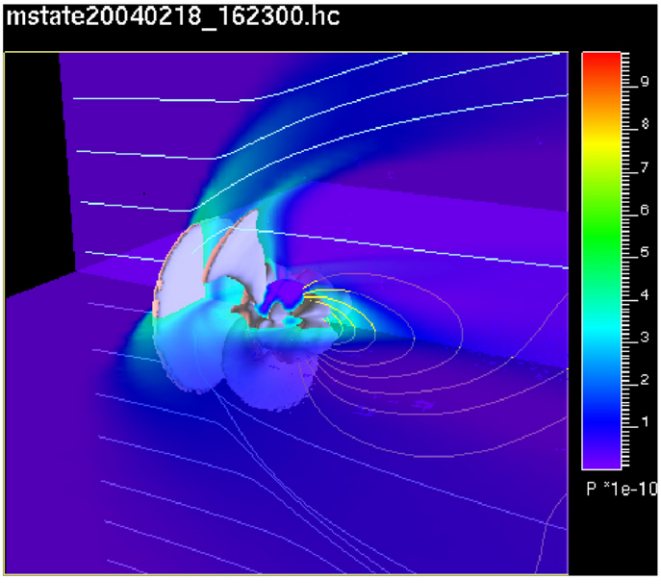

Fig. 1. A 3-D view of the magnetosphere in two cut planes visualised with `hcvis`. Pressure is colour coded along with a pressure isosurface drawn at 0.4 nPa. Flowlines from the solar wind boundary and traces of the night-side magnetic field are also shown. (For interpretation of the references to colour in this figure legend, the reader is referred to the web version of this article.)

2.7. Completed simulation runs

GUMICS runs made at FMI until end of 2010 are listed in Tables 1 and 2. Table 1 lists event study runs based on measured solar wind data and Table 2 lists noteworthy runs with synthetic solar wind input. For the event runs, the start and end epoch as well as a short description are given in Table 1.

Table 1
Real events simulated with GUMICS-4, i.e. the solar wind input was taken from satellite data. The start and end times of the simulations are given in the 1st and 2nd columns as UT, with a short description in the last column. All runs except the first were made at adaptation level 5 which corresponds to $0.25R_E$ minimum grid spacing.

Event start	Event end	Description
1991-07-11 00:00	1991-07-11 13:00	Storm recovery phase, adaption level 4
1998-03-28 21:05	1998-03-29 06:55	Substorm
1999-11-23 11:00	1999-11-23 15:00	Run to calculate Joule heating in the ionosphere and compare with Iridium satellites and SuperDARN
2000-04-06 14:00	2000-04-07 10:00	Storm
2001-01-16 20:00	2001-01-16 23:55	Run to investigate solar wind energy input to the magnetosphere, spatial variation of energy transfer (Palmroth et al., 2011, submitted)
2001-01-26 07:00	2001-01-26 12:00	Run to investigate solar wind energy input to the magnetosphere, spatial variation of energy transfer (Palmroth et al., 2011, submitted)
2001-08-04 11:05	2001-08-04 16:15	Run for GEM Challenge illumination research
2001-08-15 02:05	2001-08-15 10:00	Substorm (Palmroth et al., 2004a)
2001-08-21 07:35	2001-08-21 15:00	Run to investigate FAC
2001-08-31 00:00	2001-08-31 23:59	Run for GEM Challenge illumination research
2001-09-08 17:00	2001-09-08 23:00	Substorm
2001-10-22 06:05	2001-10-22 16:45	Storm main phase
2002-05-11 08:30	2002-05-11 11:00	Storm
2002-11-09 17:00	2002-11-09 19:00	Double fast forward shock event (Andréeová et al., 2008)
2004-02-18 14:00	2004-02-19 00:00	Run to investigate plasmaoid formation in substorm sequence (Honkonen et al., 2011)
2005-05-21 03:00	2005-05-21 10:00	Run to see general circumstances during an FTE event observed at Geotail and Cluster
2005-07-17 00:30	2005-07-17 02:30	Magnetic cloud observed by ACE, SOHO and Wind solar wind monitors on 17 July 2005 (Juusola et al., 2010)
2005-08-31 09:50	2005-09-01 11:25	GEM 2008-9 challenge
2005-12-03 16:00	2005-12-03 16:00	Substorm
2005-12-28 18:35	2005-12-29 00:00	Substorm
2006-12-14 12:29	2006-12-15 02:59	GEM 2008-9 challenge
2007-03-17 16:53	2007-03-17 20:31	Supermagnetosonic jet observed at the downstream region of a collisionless quasi-parallel shock (Hietala et al., 2009)

Table 2
Sets of GUMICS-4 runs with synthetic, idealised solar wind input. All runs were made at adaptation level 5 which corresponds to $0.25R_E$ minimum grid spacing. Most runs are also available at adaptation level 4 ($0.5R_E$ minimum spacing) for comparison.

Run title	Duration	Number	Description
IMF rotation	Various	13	IMF rotation runs with various parameters
Dipole tilt	3 h	9	IMF B_z flip with different dipole tilt angles
Constant IMF	1.5 h	10	Constant solar wind runs
Shock simulations	3 h	4	Shock simulations
Fast IMF rotation	1–4 h	45	Tail twisting runs with fast IMF turnings (Kullen and Janhunen, 2004)

3. Quantitative analysis methods

The primary scientific driver for the studies carried out using the GUMICS-4 simulation has been the global energetics of the near-Earth system. Several quantitative analysis methods for the simulation results have been developed to address this theme. The method attempt to evaluate parameters that can be used to infer information e.g. about global energy transfer questions. For instance, the different plasma domains within the near-Earth space are not always predicted to the right place at the right time by the various global MHD simulations, and hence direct *in situ* comparisons with spacecraft recordings are not always providing the best means to verify the code performance. In some cases the spacecraft recordings can be taken as global indicators, as for instance the cusp gives direct evidence of the global energetics as its location is determined by the balance of the dayside magnetic flux erosion rate and the rate at which the nightside magnetic flux returns to the dayside. Palmroth et al. (2001) investigated the GUMICS-4 cusp position as driven by the solar wind conditions and found that the Polar spacecraft measurements of the cusp location are generally in good agreement with the simulation results.

3.1. Magnetopause

Concerning global energetics, an important new methodology was identified by Palmroth et al. (2003). They determined the magnetospheric energy input directly using the GUMICS-4 simulation during a magnetic storm event that occurred on April 6–7, 2000. The method was based on identifying the magnetopause surface from the simulation for each time instant, after which the total energy flux component perpendicular to the surface was computed from the simulation. Fig. 2 shows an example of a surface identified using the method, while the colour coding shows the perpendicular total energy flux on the surface by negative (positive) colours representing inward (outward) energy flow. The surface is taken at an instant during which the IMF is purely southward. The large energy transfer from the solar wind into the magnetosphere is shown by large negative values at the tail lobes behind the cusps, while the reconnection region shows as positive values at the dayside. The energy transfer locations and IMF dependence were explained by Poynting flux focussing allowed by the open field line advection towards the tail reconnection region. By summing all energy transfer values at each instantaneous surface, a total estimate of the energy transfer per time unit is obtained. In all runs carried out and analysed in light of the energy transfer, this time series resembles the time series of the ϵ parameter, while some dissimilarities are also observed. These discrepancies are mainly due to changes in the solar wind

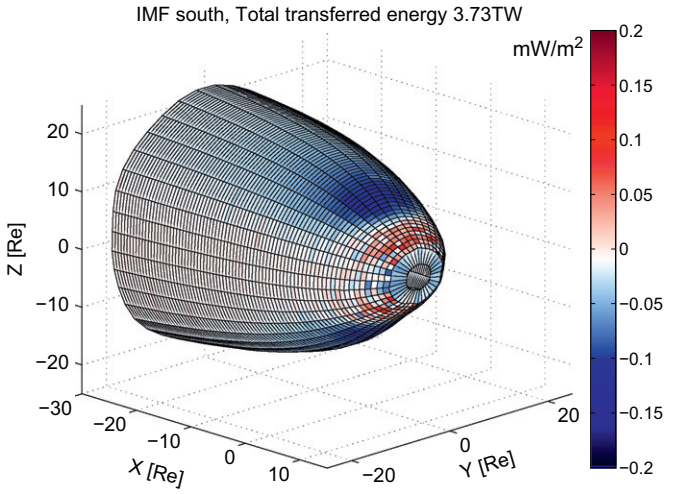

Fig. 2. Magnetopause surface coloured by the value of the passing through energy flux at one time instant in GUMICS-4. (For interpretation of the references to colour in this figure legend, the reader is referred to the web version of this article.)

dynamic pressure which is represented in the ϵ parameter only by the velocity component, and by a hysteresis effect arising from the accumulation of tangential magnetic flux at the magnetopause (Palmroth et al., 2010).

3.2. Ionosphere

The global energy investigations have also been complemented by studies of ionospheric energy dissipation (Palmroth et al., 2004a). The ionospheric energy dissipation has two major components, Joule heating and electron precipitation, and with suitable approximations both can be inferred from the GUMICS-4 simulation. Joule heating is typically formulated by the product of Pedersen conductivity and the square of the electric field, which neglects the contribution of neutral winds. Palmroth et al. (2005) computed the Joule heating from the GUMICS-4 simulation, and compared the results with observations, where the Pedersen conductivity was indirectly inferred from Polar spacecraft UVI instrument images, and the electric field was obtained from the SuperDARN radar system. The simulation was shown to be locally compatible with the observations, and the temporal variation agreed with the observations; however, the magnitude of the Joule heating was smaller than the observations indicated. Similarly, Palmroth et al. (2006) computed the electron precipitation energy in the simulation ionosphere and compared the results with auroral energy estimates derived from Polar UVI observations. Again, the spatial and temporal variations agreed with the observations, but the magnitude of the precipitation energy was smaller than that estimated from the observations. Since ionospheric Joule heating and precipitation energy flux are not too accurately known from observations in various geophysical conditions, rigorous fitting of GUMICS-4 modelling parameters to observations has not been attempted.

3.3. Locating and quantifying reconnection

Another significant boundary surface in the magnetosphere, in addition to the magnetopause, is the magnetotail neutral sheet. The neutral sheet location was determined from GUMICS-4 simulations by Laitinen et al. (2005) as the surface $z(x,y)$ where $B_x(z)$ changes sign. Fig. 3 shows magnetic reconnection energy flux on the dayside magnetopause (top panels) and on a portion of the tail neutral sheet (bottom panels). The magnetopause is

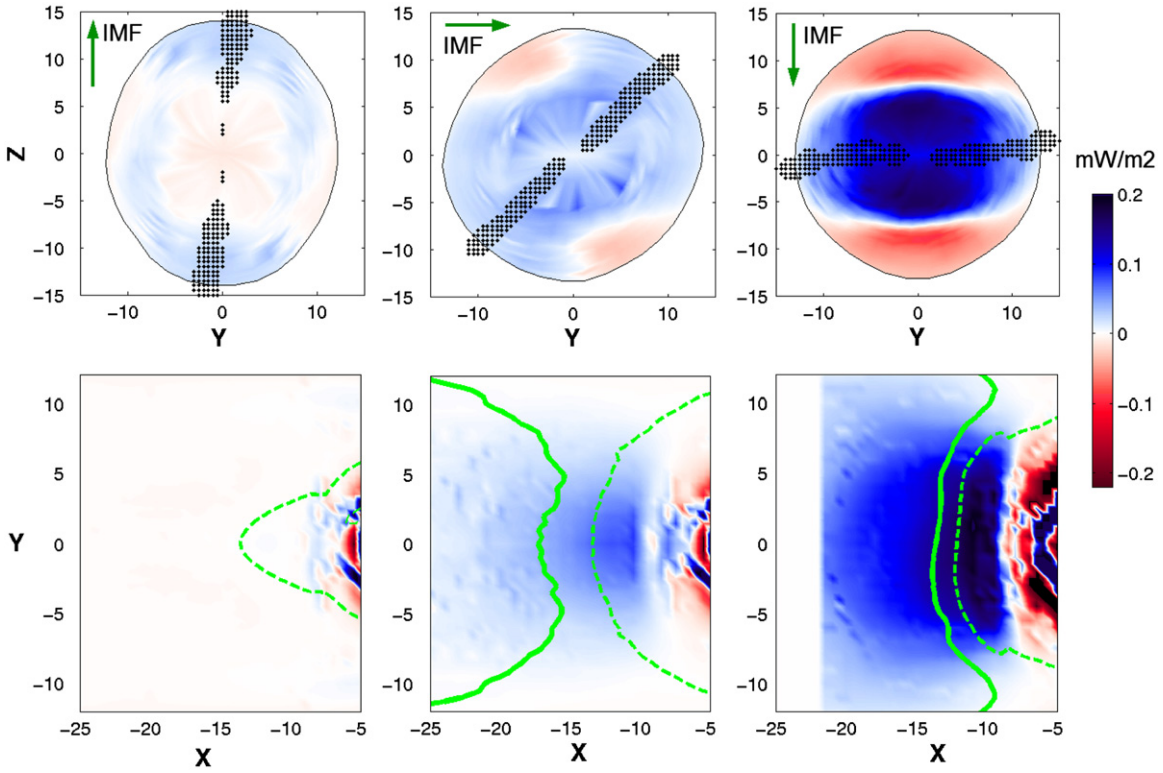

Fig. 3. Illustration of the reconnection regions in a synthetic GUMICS-4 simulation run. The dayside magnetopause (upper panels, viewed from the Sun) and the magnetotail neutral sheet (lower panels, viewed from north) are shown at three instants with northward, duskward and southward IMF (green arrows). Colouring represents the energy conversion surface density, shown with the same colour scale on both surfaces. On the magnetopause the black dots represent the approximate location of the global separator line. On the neutral sheet the solid green line is the magnetic *x*-line and the dashed green line is the plasma flow reversal line. (For interpretation of the references to colour in this figure legend, the reader is referred to the web version of this article.)

viewed from the Sun and the neutral sheet from the north as projections on the *yz* and *xy* planes, respectively. The surfaces are shown during three different IMF conditions: northward (left), duskward (middle) and southward (right). The location of the magnetopause reconnection line was estimated by searching for points (black dots in Fig. 3) where closed, semiopen and fully open magnetic field lines are present in close proximity to each other (Laitinen et al., 2006). On the magnetotail neutral sheet, the dashed green line shows the plasma flow reversal line, determined from the sign change of the plasma velocity component along the intersection of the neutral sheet and the *xz* plane. The solid green line is the magnetic *X*-line, defined by the sign change of the magnetic field component normal to the neutral sheet. During northward IMF (leftmost panel) the *X*-line is farther in the tail, outside the plot.

Contrary to what one would naively expect based on ideal MHD, the two neutral lines (magnetic *X*-line and the flow reversal line) on the magnetotail current sheet do not coincide in GUMICS (Laitinen et al., 2005). The magnetic *X*-line appears tailward of the flow reversal, the more so the thicker and quieter the plasma sheet is. Recently, a potential explanation was found by Murphy et al. (2010) who predict from their analytic model a separation of the *X*-line and the flow reversal line whenever symmetry is broken by external conditions.

To quantify reconnection, the divergence of the Poynting vector is calculated in the reconnection region (Laitinen et al., 2006). In steady state it is equal to the dissipation rate of electromagnetic energy (with a minus sign). In Fig. 3, the blue colouring represents the energy conversion surface density, $\sigma_{\mathrm{rec}} = -\int \nabla \cdot \mathbf{S}\, dn$, where $\mathbf{S} = \mathbf{E} \times \mathbf{B}/\mu_0$ is the Poynting vector and the integration is carried out along the normal $\hat{n}$ of the surface (Laitinen et al., 2006). Both on the tail current sheet and on the subsolar magnetopause, energy conversion is practically nonexistent during northward IMF, but takes place over a wide region during southward IMF. During strong tail reconnection, the neutral sheet tends to become so warped tailward of the reconnection region that it cannot be expressed as a single-valued function $z(x,y)$ which is the reason for missing data for $x < -21$ in the last panel of Fig. 3. Energy conversion is strongest not directly at the reconnection line, but near it, where plasma is accelerated by newly reconnected, kinked field lines.

Reconnection in GUMICS-4 resembles a large Sweet–Parker type diffusion region. Adjacent shock fronts that are part of models of faster reconnection have not been found in the simulations. The energy conversion surface density in the reconnection region allows one to estimate the order of magnitude of the effective magnetic Reynolds number in the simulation as $\mathcal{R}_m \sim 100$ (Laitinen et al., 2006). The reconnection rate is mainly controlled by the IMF and the solar wind velocity. It does not show spontaneous, bursty behaviour (Laitinen et al., 2007).

4. General properties of GUMICS-4 solutions

4.1. Magnetopause: GUMICS-4 versus empirical models

Fig. 4 shows the dayside last closed magnetic field lines in GUMICS and the Shue et al. (1998) and Lin et al. (2010) empirical models with identical solar wind parameters. Solar wind parameters are taken from GUMICS at (x, 60, 60) R_E, where x is the coordinate of the last closed dayside field line in GUMICS at that time. Fig. 4 shows GUMICS results from every time step from the 17 event simulations in Table 1 with the corresponding value of the empirical models. Largely, the GUMICS magnetopause lies at

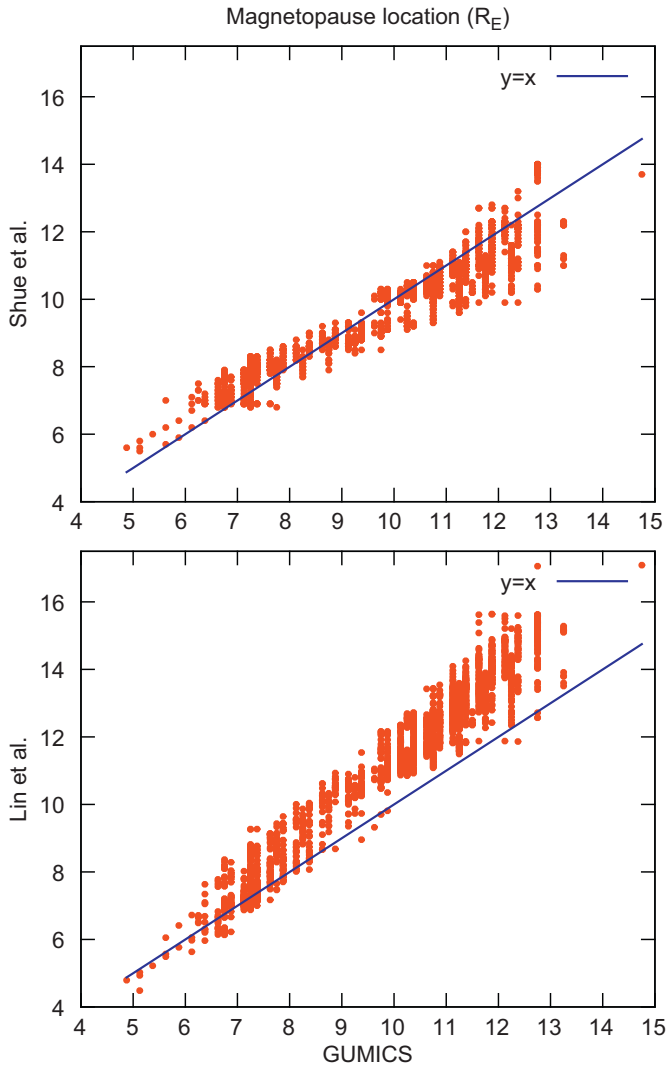

Fig. 4. Top: the dayside last closed magnetic field lines in GUMICS and the Shue et al. (1998) models with identical solar wind parameters. Solar wind parameters are taken from GUMICS at $(x, 60, 60)$ R_E, where x is the last closed dayside field line in GUMICS at that time. Shown are GUMICS results from every time step of 16 event simulations listed in Table 1. Bottom: Same but for the magnetopause model of Lin et al. (2010).

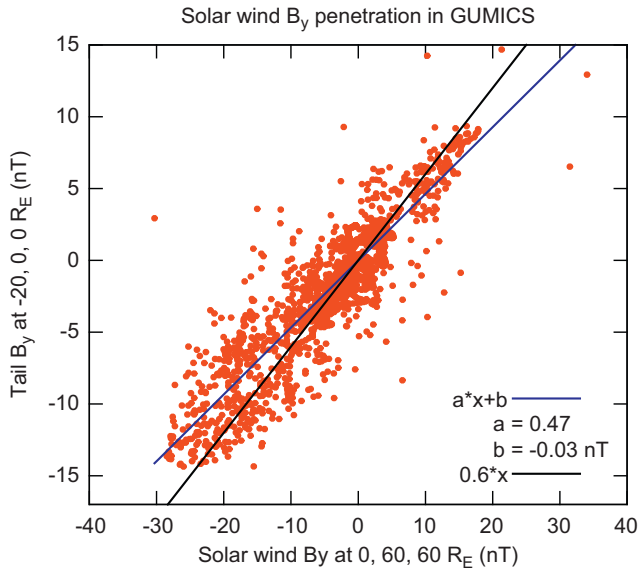

Fig. 5. GUMICS-4 solar wind B_y penetration into the magnetotail in 17 event simulations of Table 1. Blue line is a linear fit and black line shows the B_y penetration value from Sergeev (1987) (For interpretation of the references to colour in this figure legend, the reader is referred to the web version of this article.)

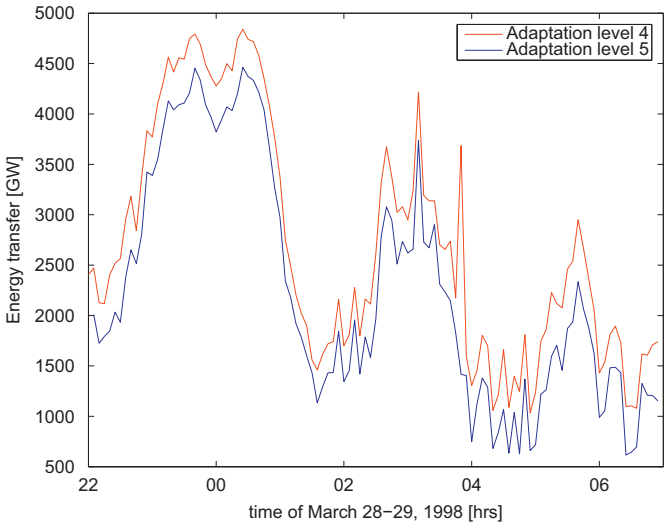

Fig. 6. Input power through the magnetopause as computed from GUMICS for March 28–29, 1998, for adaptation levels 4 and 5. (For interpretation of the references to colour in this figure legend, the reader is referred to the web version of this article.)

least statistically in-between the two empirical models in cases where the empirical models differ from each other.

4.2. Penetration of IMF B_y into the tail

Fig. 5 shows the GUMICS solar wind B_y penetration into the magnetotail in 17 event simulations listed in Table 1. In GUMICS about 50% of the solar wind B_y taken from (0, 60, 60) R_E penetrates into the magnetotail at $(-20, 0, 0)$ R_E. Sergeev (1987) investigated IMF B_y penetration into the magnetotail based on ISEE-1 measurements and found that on average about 60% of IMF B_y penetrates into the magnetotail on various distances along the x-axis. Thus, GUMICS-4 agrees well with observations regarding IMF penetration into the magnetotail.

4.3. Effect of grid adaptation level

Fig. 6 shows an example of the energy transfer through the magnetopause during a pair of substorms that occurred on March 28–29, 1998. Solar wind data were used as input to the code in the sunward wall of the simulation box, and two runs with different grid spacing were carried out. Red trace shows the energy transfer through the magnetopause using adaptation level 4, where the smallest grid spacing is $0.5R_E$. Blue trace uses adaptation level 5, where the smallest grid spacing is $0.25R_E$. The enhancements in the energy input occur during southward IMF that allows low latitude reconnection and Poynting flux focussing. The small difference between the results obtained from the two runs with different grid resolutions illustrate the good quality of the simulation itself as well as the method for searching the magnetopause and computing the energy input through the surface.

The effect of grid resolution in the magnetotail reconnection region is illustrated in Fig. 7. The first panel shows the tail reconnection power, i.e. the net flux of the Poynting vector into

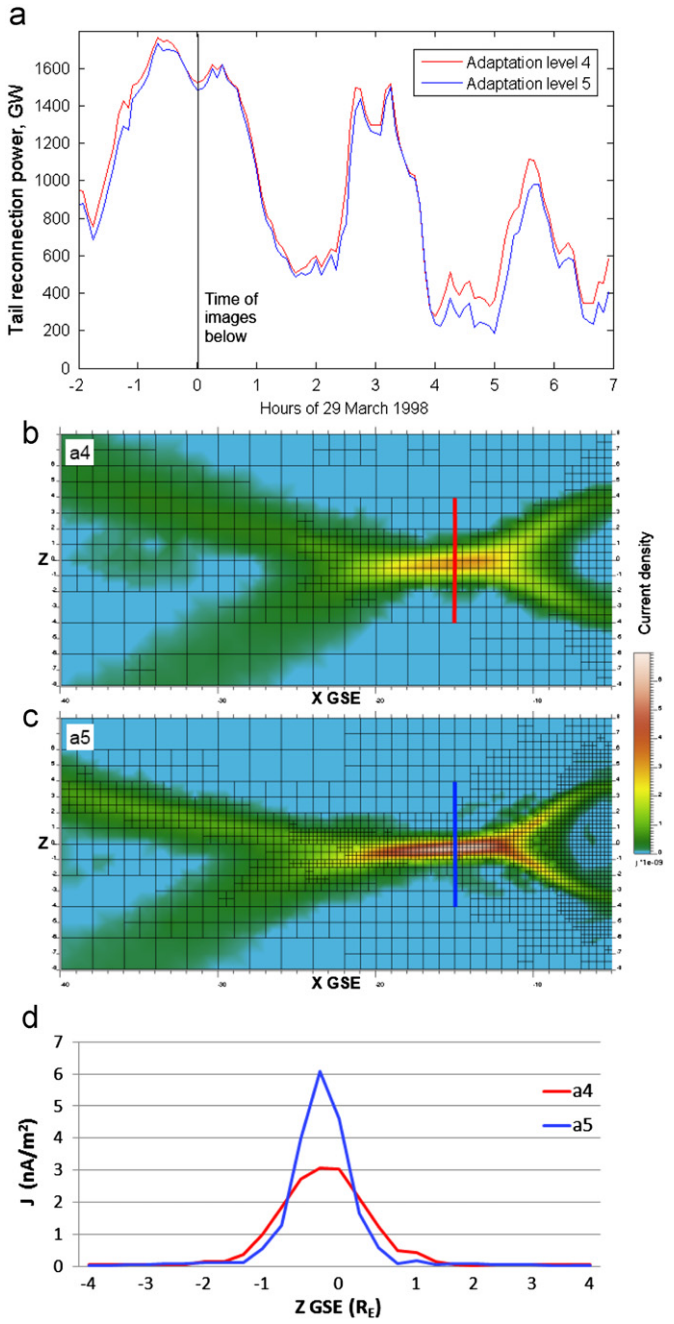

Fig. 7. (a) Magnetotail reconnection power (energy conversion rate) as a function of time in two simulation runs with the same solar wind input but different maximum grid resolutions. At adaptation level a4 the best resolution is $0.5R_E$ and at adaptation level a5 it is $0.25R_E$. (b) Current density in the near-Earth magnetotail current sheet region at a4. Shown is the plane $y=0$, $-40<x<-5$, $-8<z<8$. The grid is also drawn. (c) Same as (b) but using data from the better resolution run a5. (d) Current density profile of the magnetotail current sheet at $x=-15$, $y=0$ in the two runs. The data are taken along the red and blue lines in panels (b) and (c). (For interpretation of the references to colour in this figure legend, the reader is referred to the web version of this article.)

the box $-30<x<-10$, $-10<y<10$ and $-6<z<6$, a volume encompassing the thin current sheet region in the tail (Laitinen et al., 2005). The curves follow each other very closely, just like in the magnetopause energy transfer case (Fig. 6). The smaller adaptation level (larger grid size) produces slightly higher values for both quantities. The difference is constant rather than relative, suggesting that a larger grid size allows, probably through enhanced diffusion, a somewhat larger "background" value of energy flow and conversion in the simulation. The physical processes caused by solar wind variations then appear as similar and equally large variations in these integrated quantities regardless of the resolution. However, the "background" and differences in it are small compared to the dynamic range of the quantities.

Panels b and c in Fig. 7 show a cross-cut of the thin current sheet region on the $y=0$ plane. The colouring represents the total current density while the grid is drawn with black lines. The basic structure of the tail is similar in both runs. However, a clear difference is seen in the thin current sheet region between $-20<x<-10$: the maximum current density in the adaptation level 5 run is twice as large as in the adaptation level 4 run. This is further illustrated by the current density profiles in panel d. They also show that the current sheet is slightly thicker in the lower resolution run. Even farther in the tail the current sheet is thinner and current density larger in the adaptation level 5 run. This is natural since the current density is a gradient of the magnetic field so halving the grid size in practice halves the minimum spatial extent that a given change in a variable value needs (in this case, the change in B_x from one lobe to the other). Increasing resolution sharpens the gradients and increases current densities also elsewhere e.g. at the magnetopause (not shown). Away from the boundary regions the resolution effect on variable values is minor: for example, the maximum lobe magnetic field strength at $x=-20$ is about 10% larger at adaptation level 5 than at adaptation level 4.

We conclude that adaptation level 5 provides adequate resolution for most studies on the global dynamics of the magnetosphere, as comparison with a lower resolution run does not show significant differences in the structure of the magnetosphere or in the magnitudes or temporal behaviour of integrated quantities describing energy flow in the system. The grid limits the accuracy of representation of thin boundaries, wherefore local variable values, especially gradient quantities, at such boundaries may be unrealistic and should be compared with observations only with great care. It is advisable to base analysis on spatially integrated quantities whereby the effects of boundary thickness and local details are removed. In spite of the grid-induced local effects, differences in the global energy flow in the system are negligible between the runs with different resolutions. We have also experimented with altered spatial distributions of cell refinements and gotten the same result: local effects can be large, global ones are negligible. This indicates that the integrated quantities used for energy flow analysis represent true physical properties of the solution and are not dependent on the grid resolution. If a need for more accurate results beyond adaptation level 5 would arise, one might have to consider whether one would need to add some beyond-MHD physics in specific regions of the magnetosphere.

4.4. Ionospheric field-aligned current and precipitation energy flux

Fig. 8 presents a comparison of observations and GUMICS simulation results of ionospheric field-aligned currents (FAC). Panels a and c are GUMICS results on the FAC during northward and southward IMF, respectively, while panels b and d are statistics based on the CHAMP spacecraft observations (Juusola et al., 2009). Blue (red) colours illustrate upward (downward) FAC. Both the GUMICS results and the CHAMP statistics for northward IMF show the average current at times of IMF clock angle between $\theta>300^\circ$ and $\theta<60^\circ$ during which lobe reconnection should be operating. The GUMICS results were time averaged from a synthetic run where the IMF direction rotates slowly. Similarly, the southward IMF results include orientations that are within 60° from the due south direction. In the simulation results, the solar wind dynamic pressure is steadily 2 nPa, while

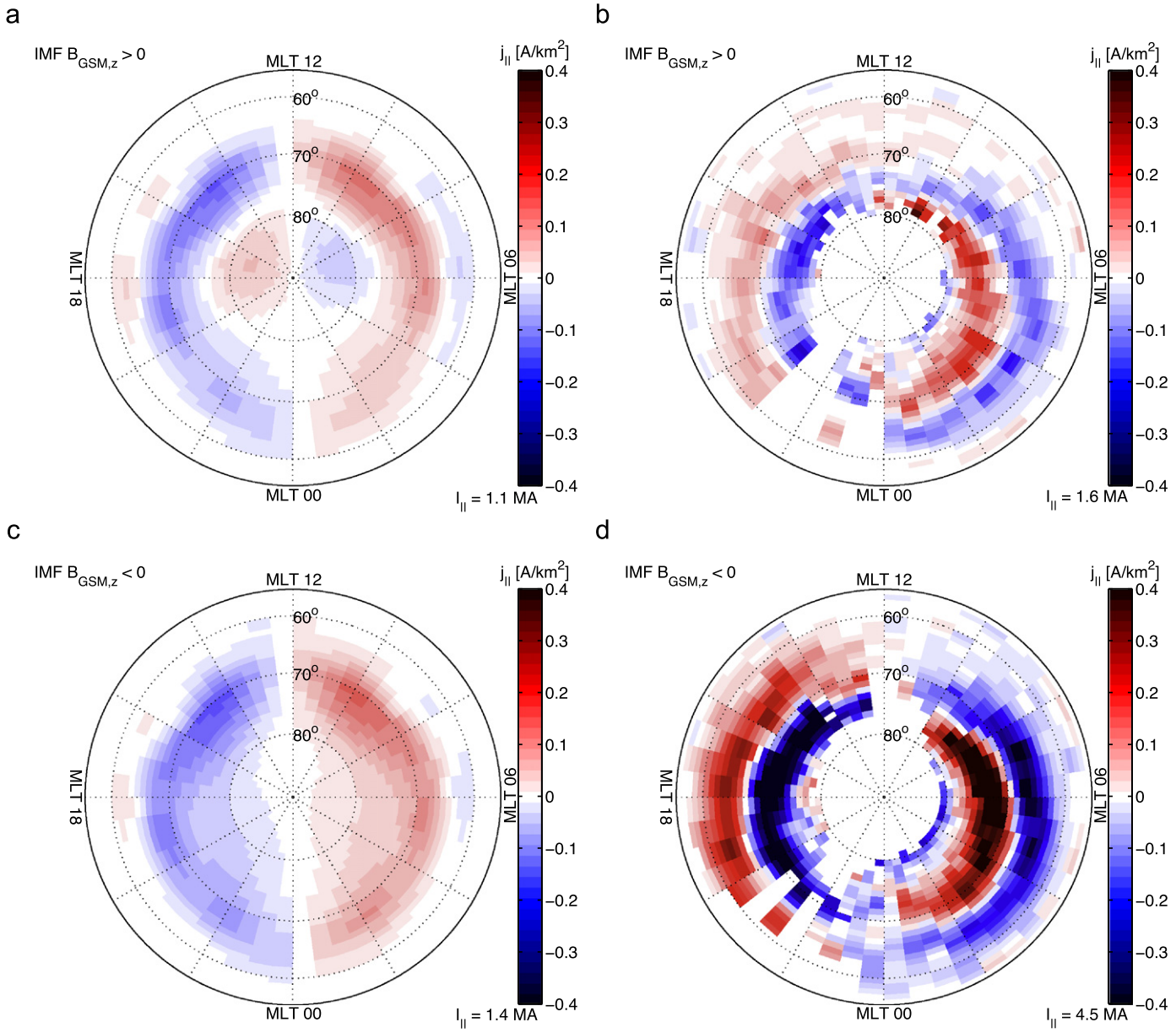

Fig. 8. GUMICS-4 (left) field-aligned current pattern compared to statistical CHAMP satellite results (right), for positive (top) and negative (bottom) IMF (For interpretation of the references to colour in this figure legend, the reader is referred to the web version of this article.)

the CHAMP results are gathered during a variety of dynamic pressure conditions, of which the vast majority range between 1 and 3 nPa. The gap around the magnetic pole in the CHAMP statistics is due to the method by which the FAC was computed from the satellite magnetic field measurements (in each satellite pass, the FAC was assumed to be a function of latitude only).

Fig. 8a shows that the GUMICS model produces a roughly comparable magnitude for the FAC as compared to the CHAMP statistics (Fig. 8b). The CHAMP statistics do not show the NBZ current system originating from lobe reconnection due to the technique of inferring the FAC, while the GUMICS results show an enhancement of FAC at roughly the right location. The Region 1 current system in the simulation is located somewhat equatorward of that given by the CHAMP statistics. The Region 2 currents in GUMICS are virtually nonexistent, maybe due to the lack of the plasma pressure in MHD which in the nature is created by the high-energy ring current population. This is a known feature and present in other codes as well. In GUMICS, the modelling of Region 2 current system is somewhat improved when increasing the magnetospheric grid resolution, as then the pressure gradient within the inner magnetosphere is sharper allowing a better representation of the Region 2 system as well. Furthermore, while the spatial coverage of the current system is on average similar to the observed one, the current continuation over the noon-midnight meridian in the day-side is not reproduced as well.

During southward IMF (Fig. 8c and d), GUMICS does not produce as intense currents as are present in the CHAMP statistics. The FAC intensity in GUMICS is also a strong function of the solar wind dynamic pressure (Palmroth et al., 2004b). Again, the Region 1 currents are spread over a larger area in GUMICS than in the CHAMP statistics, while the Region 2 currents do not appear in the large scale. We suspect that the reason is the inner magnetospheric modelling, as adding Region 2 currents to the modelling might also push the Region 1 currents closer to the pole thus improving the agreement.

5. Conclusions and future prospects

GUMICS-4 is a mature ionosphere–magnetosphere coupling and global MHD simulation which in many cases produces results that are in good agreement with observations. Examples where the agreement is good include the magnetopause location and the amount of IMF B_y penetration in the magnetotail.

Being an MHD-based model, however, GUMICS-4 has some limitations. In particular, the near-Earth region is not accurately modelled, because in reality it consists of overlapping hot and cold plasma populations, but single-fluid MHD must necessarily approximate it with a single temperature. Also the physics of magnetotail reconnection is incomplete in GUMICS because the Hall term and electron pressure term are not included.

GUMICS-4 can be successfully run on a single-processor personal computer environment. This is due to its innovative use of temporal subcycling and semiautomatic adaptive cell-by-cell gridding. Unlike some other global MHD simulations, GUMICS does not make use of an artificially lowered speed of light (Boris correction) for speeding up the computations. Even though the GUMICS MHD solver is only first order in spatial accuracy, the produced current sheets and magnetopause appear sharp, being not much wider than one grid spacing. Runs made at different adaptation levels indicate that the results are grid converged in terms of many output quantities.

A parallel version of GUMICS-4 is currently under development. We expect the parallel version to allow a much increased computing speed which in turn enables investigations with a higher adaptation level and/or reduced inner boundary distance which will likely contribute towards improved modelling of the Region-2 current systems.

Acknowledgements

Part of the research leading to these results has received funding from the European Research Council under the European Community's Seventh Framework Programme (FP7/2007-2013)/ ERC Starting Grant agreement number 200141-QuESpace. The work of MP, IH and TL is supported by the Academy of Finland. Gábor Facskó was supported by the OTKA Grant K75640 of the Hungarian Scientific Research Fund. We acknowledge useful information exchange with Tamas Gombosi at the time when GUMICS and SWMF were both developed. The operational support of the CHAMP mission by the German Aerospace Center (DLR) and the financial support for the data processing by the Federal Ministry of Education (BMBF), as part of the Geotechnology Programme, are gratefully acknowledged.

References

Andréeová, K., Pulkkinen, T.I., Laitinen, T.V., Přech, L., 2008. Shock propagation in the magnetosphere: observations and MHD simulations compared. Journal of Geophysical Research 113, A09224. http://dx.doi.org/10.1029/2008JA013350.

Axford, W.I., Hines, C.O., 1961. A unifying theory of high-latitude geophysical phenomena and geomagnetic storms. Canadian Journal of Physics 39, 1433.

Birn, J., Drake, J.F., Shay, M.A., Rogers, B.N., Denton, R.E., Hesse, M., Kuznetsova, M., Ma, Z.W., Bhattacharjee, A., Otto, A., Pritchett, P.L., 2001. Geospace Environmental Modeling (GEM) reconnection challenge. Journal of Geophysical Research 106, 3715.

Brackbill, J.U., Barnes, D.C., 1980. The effect of nonzero product of magnetic gradient and B on the numerical solution of the magnetohydrodynamic equations. Journal of Computational Physics 35, 426–430.

De Zeeuw, D.L., Sazykin, S., Wolf, R.A., Gombosi, T.I., Ridley, A.J., Toth, G., 2004. Coupling of a global MHD code and an inner magnetospheric model: initial results. Journal of Geophysical Research 109, A12219. http://dx.doi.org/10.1029/2003JA010366.

Dungey, J.R., 1961. Interplanetary magnetic field and the auroral zones. Physical Review Letters 6, 47.

Harten, A., Lax, P.D., van Leer, B., 1983. On upstrean differencing and Godunov-type schemes for hyperbolic conservation laws. SIAM Review 25, 35–61.

Hedin, A.E., 1991. Extension of the MSIS thermospheric model into the middle and lower atmosphere. Journal of Geophysical Research 96, 1159–1172.

Hietala, H., Laitinen, T.V., Andréeová, K., Vainio, R., Vaivads, A., Palmroth, M., Pulkkinen, T.I., Koskinen, H.E.J., Lucek, E.A., Rème, H., 2009. Supermagnetosonic jets behind a collisionless quasiparallel shock. Physical Review Letters 103. (p. id. 245001).

Honkonen, I., Palmroth, M., Pulkkinen, T.I., Janhunen, P., Aikio, A., 2011. On large plasmoid formation in a global magnetohydrodynamic simulation. Annales Geophysicae 29, 167–179.

Janhunen, P., Huuskonen, A., 1993. A numerical ionosphere–magnetosphere coupling model with variable conductivities. Journal of Geophysical Research 98, 9519–9530.

Janhunen, P., Pulkkinen, T.I., Koskinen, H.E.J., July 12, 1995. Simulating Semiglobal Magnetosphere–Ionosphere Coupling with Applications to Auroral Phenomena, Poster Presentation GAB31H-03 in IAGA/IUGG, Boulder, Colorado.

Janhunen, P., 1996. GUMICS-3 – a global ionosphere–magnetosphere coupling simulation with high ionospheric resolution. In: Burke, W., Guyenne, T.-D. (Eds.), Environment Modelling for Space-based Applications, Symposium Proceedings (ESA SP-392). ESTEC, Noordwijk, pp. 233. (18–20 September).

Janhunen, P., 2000. A positive conservative method for magnetohydrodynamics based on HLL and Roe methods. Journal of Computational Physics 160, 649–661.

Juusola, L., Kauristie, K., Amm, O., Ritter, P., 2009. Statistical dependence of auroral ionospheric currents on solar wind and geomagnetic parameters from 5 years of CHAMP satellite data. Annales Geophysicae 27 (3), 1005–1017.

Juusola, L., Andréeová, K., Amm, O., Kauristie, K., Milan, S.E., Palmroth, M., Partamies, N., 2010. Effects of a solar wind dynamic pressure increase in the magnetosphere and in the ionosphere. Annales Geophysicae 28, 1945–1959.

Kullen, A., Janhunen, P., 2004. Relation of polar auroral arcs to magnetotail twisting and IMF rotation: a systematic MHD simulation study. Annales Geophysicae 22, 951–970.

Laitinen, T.V., Pulkkinen, T.I., Palmroth, M., Janhunen, P., Koskinen, H.E.J., 2005. The magnetotail reconnection region in a global MHD simulation. Annales Geophysicae 23, 3753–3764.

Laitinen, T.V., Janhunen, P., Pulkkinen, T.I., Palmroth, M., Koskinen, H.E.J., 2006. On the characterization of magnetic reconnection in global MHD simulations. Annales Geophysicae 24, 3059–3069.

Laitinen, T.V., Palmroth, M., Pulkkinen, T.I., Janhunen, P., Koskinen, H.E.J., 2007. Continuous reconnection line and pressure-dependent energy conversion on the magnetopause in a global MHD model. Journal of Geophysical Research 112, A11201. http://dx.doi.org/10.1029/2007JA012352.

Lin, R.L., Zhang, X.X., Liu, S.Q., Wang, Y.L., Gong, J.C., 2010. A three-dimensional asymmetric magnetopause model. Journal of Geophysical Research 115, A04207. http://dx.doi.org/10.1029/2009JA014235.

Lotko, W., Schultz, C.G., October 14–16, 1987. Internal shear layers in auroral dynamics. In: Modeling magnetospheric plasma, Proceedings of the First Huntsville Workshop on Magnetosphere/Ionosphere Plasma Models, Guntersville, Alabama, pp. 121–132.

Lyon, J.G., Fedder, J.A., Mobarry, C.M., 2004. The Lyon–Fedder–Mobarry (LFM) global MHD magnetospheric simulation code. Journal of Atmospheric and Solar-Terrestrial Physics 66, 1333–1350.

Moen, J., Brekke, A., 1993. The solar flux influence on quiet time conductances in the auroral ionosphere. Geophysical Research Letters 20, 971–974.

Murphy, N.A., Sovinec, C.R., Cassak, P.A., 2010. Magnetic reconnection with asymmetry in the outflow direction. Journal of Geophysical Research 115, A09206. http://dx.doi.org/10.1029/2009JA015183.

Ogino, T., Walker, R.J., Ashour-Abdalla, M., 1994. A global magnetohydrodynamic simulation of the response of the magnetosphere to a northward turning of the interplanetary magnetic field. Journal of Geophysical Research 99, 11027–11042.

Palmroth, M., Janhunen, P., Pulkkinen, T.I., Peterson, W.K., 2001. Cusp and magnetopause locations in global MHD simulation. Journal of Geophysical Research 106, 29,435–29,450.

Palmroth, M., Pulkkinen, T.I., Janhunen, P., Wu, C.-C., 2003. Stormtime energy transfer in global MHD simulation. Journal of Geophysical Research 108 (A1), 1048. http://dx.doi.org/10.1029/2002JA009446.

Palmroth, M., Janhunen, P., Pulkkinen, T.I., Koskinen, H.E.J., 2004a. Ionospheric energy input as a function of solar wind parameters: global MHD simulation results. Annales Geophysicae 22, 549–566.

Palmroth, M., Pulkkinen, T.I., Janhunen, P., McComas, D.J., Smith, C., Koskinen, H.E.J., 2004b. Role of solar wind dynamic pressure in driving ionospheric Joule heating. Journal of Geophysical Research 109, A11302. http://dx.doi.org/10.1029/2004JA010529.

Palmroth, M., Janhunen, P., Pulkkinen, T.I., Aksnes, A., Lu, G., Ostgaard, N., Watermann, J., Reeves, G.D., Germany, G.A., 2005. Assessment of ionospheric Joule heating by GUMICS-4 MHD simulation, AMIE, and satellite-based statistics, Towards a synthesis. Annales Geophysicae 23, 2051–2068.

Palmroth, M., Janhunen, P., Germany, G.A., Lummerzheim, D., Liou, K., Baker, D.N., Barth, C., Weatherwax, A.T., Watermann, J., 2006. Precipitation and total power consumption in the ionosphere, Global MHD simulation results compared with Polar and SNOE observations. Annales Geophysicae 24, 861–872.

Palmroth, M., Koskinen, H.E.J., Pulkkinen, T.I., Toivanen, P.K., Janhunen, P., Milan, S.E., Lester, M., 2010. Magnetospheric feedback in solar wind energy transfer. Journal of Geophysical Research 115, A00I10. http://dx.doi.org/10.1029/2010JA015746.

Powell, K.G., Roe, P.L., Linde, T.J., Gombosi, T.I., De Zeeuw, D.L., 1999. A solution-adaptive upwind scheme for ideal magnetohydrodynamics. Journal of Computational Physics 154, 284–309.

Press, W.H., Teukolsky, S.A., Vetterling, W.T., Flannery, B.P., 1992. Numerical Recipes in C The art of scientific computing. 2nd ed., Cambridge.

Pulkkinen, A., Rastätter, L., Kuznetsova, M., Hesse, M., Ridley, A., Raeder, J., Singer, H.J., Chulaki, A., 2010. Systematic evaluation of ground and geostationary magnetic field predictions generated by global magnetohydrodynamic models. Journal of Geophysical Research 115, A03206. http://dx.doi.org/10.1029/2009JA014537.

Raeder, J., Larson, D., Li, W., Kepko, E.L., Fuller-Rowell, T., 2008. OpenGGCM simulations for the THEMIS mission. Space Science Reviews 141, 535. http://dx.doi.org/10.1007/s11214-008-9421-5.

Ridley, A.J., Gombosi, T.I., Sokolov, I.V., Tóth, G., Welling, D.T., 2010. Numerical considerations in simulating the global magnetosphere. Annales Geophysicae 28, 1589–1614.

Roe, P.L., 1981. Approximate Riemann solvers, parameter vectors, and difference schemes. Journal of Computational Physics 43, 357–372.

Sergeev, V.A., 1987. Penetration of the by component of the IMF into the magnetotail. Geomagnetism i Aeronomiia 27, 612–615. (in Russian).

Shue, J.-H., Song, P., Russell, C.T., Steinberg, J.T., Chao, J.K., Zastenker, G., Vaisberg, O.L., Kokubun, S., Singer, H.J., Detman, T.R., Kawano, H., 1998. Magnetopause location under extreme solar wind conditions. Journal of Geophysical Research 103, 17691–17700.

Tanaka, T., 1994. Finite volume TVD scheme on an unstructured grid system for three-dimensional MHD simulation of inhomogeneous systems including strong background potential fields. Journal of Computational Physics 111, 381–389.

Toffoletto, F.R., Sazykin, S., Spiro, R.W., Wolf, R.A., Lyon, J.G., 2004. RCM meets LFM: initial results of one-way coupling. Journal of Atmospheric and Solar-Terrestrial Physics 66 (15–16), 1361.

Toth, G., Sokolov, I.V., Gombosi, T.I., Chesney, D.R., Clauer, C.R., De Zeeuw, D.L., Hansen, K.C., Kane, K.J., Manchester, W.B., Oehmke, R.C., Powell, K.G., Ridley, A.R., Roussev, I.I., Stout, Q.F., Volberg, O., Wolf, R.A., Sazykin, S., Chan, A., Yu, B., Kota, J., 2005. Space weather modeling framework: a new tool for the space science community. Journal of Geophysical Research 110. http://dx.doi.org/10.1029/2005JA011126.

Wang, W., Wiltberger, M., Burns, A.G., Solomon, S.C., Killeen, T.L., Maruyama, N., Lyon, J.G., 2004. Initial results from the coupled magnetosphere–ionosphere–thermosphere model: thermosphere–ionosphere responses. Journal of Atmospheric and Solar-Terrestrial Physics 66 (15–16), 1425.